RESEARCH PAPER

Development and Evaluation of Phloretin-Loaded Transethosomal Nail Lacquer for Enhanced Transungual Delivery in Onychomycosis

Pratiksha Santosh Jadhav[1*], Trusha Shangrapawar[2], Sujit Kakade[3], Ashok Bhosale[4]

[1]Dept. of Pharmaceutics, PDEA's Shankarrao Ursal College of Pharmaceutical Sciences and Research Centre, Kharadi, Pune, Maharashtra, India.*

Email: pj494343@gmail.com

[2] Assistant Professor, Dept. of Pharmaceutics, PDEA's Shankarrao Ursal College of Pharmaceutical Sciences and Research Centre, Kharadi, Pune, Maharashtra, India.

[3]Associate Professor, Department of Pharmaceutics, PDEA's Shankarrao Ursal College of Pharmaceutical Sciences and Research Centre, Kharadi, Pune, Maharashtra, India

[4]Principle of PDEA's Shankarrao Ursal College of Pharmaceutical Sciences and Research Centre, Kharadi, Pune, Maharashtra, India.

ABSTRACT

Objectives: Onychomycosis, a chronic fungal nail infection, remains therapeutically challenging due to the formidable physicochemical barrier of the nail plate that limits penetration of conventional antifungal agents. The present study aimed to develop, optimize, and evaluate phloretin-loaded transethosomal nail lacquer for enhanced transungual delivery as a clinically viable alternative to systemic antifungal therapy.

Methods: Phloretin-loaded transethosomes were fabricated by the ethanol injection method and optimized using a three-factor, three-level Box-Behnken design with soya phosphatidylcholine concentration, isopropyl myristate concentration, and ethanol volume as independent variables, targeting minimized vesicle size and maximized entrapment efficiency. The optimized transethosomes were incorporated into ethyl cellulose-based nail lacquer formulations and evaluated for physicochemical characterization, ex vivo transungual permeation through bovine hoof membrane, accelerated stability per ICH Q1A(R2) guidelines, and in vitro antifungal activity by agar well diffusion method.

Results: The optimized formulation (PF1) achieved vesicle size of 163.4 nm, entrapment efficiency of 68.7%, and deformability index of 3.84 with desirability of 1.000. Among nail lacquer formulations, NL2 (7.5% ethyl cellulose) was selected as optimal based on balanced physicochemical profile, demonstrating steady-state flux of 7.83 µg/cm²/h, enhancement ratio of 3.54, and drug content of 97.8%. NL2 exhibited zones of inhibition of 31.4 mm and 27.8 mm against *Trichophyton rubrum* and *Candida albicans* respectively, comparable to terbinafine standard, and retained physicochemical stability with drug content of 96.3% after three months.

Conclusion: The developed phloretin transethosomal nail lacquer demonstrated superior transungual permeation, potent antifungal efficacy, and excellent stability, offering a targeted topical alternative that circumvents systemic toxicity associated with oral antifungals. These findings present a strong foundation for future in vivo pharmacokinetic evaluation and potential clinical translation.

Keywords: Onychomycosis; Phloretin; Transethosomes; Nail lacquer; Transungual drug delivery; Box-Behnken design; Antifungal activity

How to cite this article: Jadhav PS, Shangrapawar T, Sujit Kakade, Bhosale A. Formulation and Evaluation of Transethosomal NailLacquer for Enhanced Transungual Delivery of Phloretin in the Treatment of Onychomycosis. Int J Drug Deliv Technol.2026;16(64s):1087-1104. DOI: 10.25258/ijddt.16.64s.118

INTRODUCTION

Onychomycosis is the most common nail disorder in the world and is caused primarily by dermatophytes (*Trichophyton rubrum, Trichophyton mentagrophytes*), non-dermatophyte moulds, and Candida species, and is responsible for about 50% of all nail abnormalities, with nearly 10% of the world's population suffering from it [1]. Its incidence increases rapidly as age goes up and is increased in the presence of immunocompromised state, diabetes mellitus, peripheral vascular disease and long time wearing of occlusion shoes more than 30% in people above 60 years. The burden of the disease is substantial, both in terms of the loss of direct health expenditure and the loss of quality of life, physical mobility and/or occupation [2]. Systemic antifungal drugs (Oral terbinafine and itraconazole) that are clinically effective have side effects of serious hepatotoxicity, drug-drug interactions, long treatment periods ranging from 3 to 6 months, and high recurrence rates of more than 20% [3]. Although these are safer, most topical monotherapies are poorly effective due to the nail plate's formidable physicochemical barrier, which includes a dense and cross linked matrix of keratin, low water content, and highly hydrophilic nature that limits the penetration of most antifungal agents to subungual concentrations that are insufficient for therapeutic effect [4].

The long-standing clinical and pharmacokinetical constraints highlight the need for new transungual drug delivery approaches that are able to penetrate the nail barrier and achieve local efficacy [5].

Phloretin, a dihydrochalcone flavonoid glycoside aglycone mainly found in the root bark and leaves of apple (Malus domestica) and related species of the Rosaceae family, is a pharmacologically promising compound for antifungal treatment [6]. Phloretin is a compound with a molecular weight of 274.27 Da and moderate lipophilicity (log P ≈ 1.72), which has a unique chemical structure of a dihydrochalcone, with several phenolic hydroxyl groups giving it widespread biological activity [7]. It acts on fungi by disrupting cell membrane integrity, inhibiting glucose uptake through GLUT-mediated transport, blocking ergosterol biosynthesis, and possibly producing ROS which result in damage to fungal viability and proliferation. In addition to fungicidal properties, phloretin has strong anti-inflammatory, antioxidant and antiproliferative activity, which is therapeutically relevant in the inflammatory environment typical of chronic onychomycosis [8]. There is evidence published showing that phloretin is highly active against *T. rubrum* and *Candida albicans* has minimum inhibitory concentrations similar to known antifungals. But its application potential is seriously restricted due to its low aqueous solubility, rapid metabolism and poor ability to penetrate into the nail plate, requiring a high-level carrier system to make the fullest use of its pharmacological properties [9].

Transethosomes are third generation ultradeformable vesicular carrier system that has been developed by incorporation edge activators and penetration-enhancing lipids in to conventional ethosomal system, which has excellent membrane deformability along with the inherent permeation-enhancing ability of ethanol [10]. In contrast to the traditional liposomes and ethosomes, the transethosomes penetrate into the biological and structural barriers by squeezing, without any disruption of the vesicles, because of the transungual hydration gradient. The use of isopropyl myristate as a novel dual-function edge activator in the present study both fluidizes the phospholipid bilayer, and also solubilizes phloretin in the carrier matrix, thereby increasing the EE and permeation kinetics of the vesicles [11]. Such deformable vesicles when embedded into the ethyl cellulose-based nail lacquer further give a sustained release depot directly on the nail surface, and the contact time between the drug and the skin is extended; the drug washout is prevented and the drug flux is controlled on the nail surface, which is beneficial for a long therapeutic window. The scientific rationale for the present approach has been repeatedly confirmed by recent advances in the delivery of ultradeformable carrier systems into the nail [12].

The aim of the present study was to develop, optimize and evaluate phloretin loaded transethosomes entrapped in a nail lacquer to achieve improved transungual delivery in onychomycosis management. Optimization of transethosomal formulation parameters by Box-Behnken statistical design, characterization, ex vivo permeation through bovine hoof membrane, accelerated stability testing and in vitro evaluation of antifungal activity against *Trichophyton rubrum* and *Candida albicans* were among the specific objectives.

MATERIALS AND METHODS

MATERIALS

Phloretin (purity ≥98%, MW 274.27 Da) was procured from Sciquaint Innovations Pvt. Ltd. (Pune, India); soya phosphatidylcholine (pharmaceutical grade, phosphatidylcholine content ≥94%) from Lipoid GmbH (Ludwigshafen, Germany); isopropyl myristate, Span 80, dibutyl phthalate, ethyl acetate, dimethyl sulfoxide, and ethanol (all analytical grade) from Research Lab Fine Chem Industries (Mumbai, India); ethyl cellulose (standard grade, viscosity 46 cP), Tween 80, phosphotungstic acid, Sabouraud Dextrose Agar, terbinafine reference standard (purity ≥99%), and dialysis membrane (MWCO 12,000–14,000 Da) from HiMedia Laboratories Pvt. Ltd. (Mumbai, India). Bovine hoof membrane was obtained from a local government-approved slaughterhouse (Pune, India), and *Trichophyton rubrum* (ATCC 28188) and *Candida albicans* (ATCC 10231) were procured from the Microbial Type Culture Collection, Institute of Microbial Technology (Chandigarh, India). Phosphate buffer saline (pH 7.4) and normal saline (0.9% w/v NaCl) were prepared in-house. All other reagents were of analytical grade.

METHODS

Calibration Curve of Phloretin

A stock solution of phloretin (1000 µg/mL) was prepared by dissolving 10 mg in 10 mL ethanol and then working standards of 2, 4, 6, 8, 10 and 12 µg/mL were prepared by serial dilution. The absorbance of each standard was recorded at λ_{max} 284 nm on a UV-visible spectrophotometer (LABMAN Scientific Instruments Pvt. Ltd., Model LMSPUV1000B, India) with ethanol blank as blanks. The calibration curve was plotted with absorbance against concentration and the linearity was tested by linear regression analysis to get R2, slope and intercept. The equation derived was used in all subsequent studies to back-calculate the concentration of phloretin. All experiments were repeated three times (n=3) and are reported as mean ± SD [13,14].

Fourier Transform Infrared Spectroscopy

The FTIR technique was used to evaluate the physicochemical compatibility of phloretin and formulation excipients. Phloretin was gently triturated with water to give pure phloretin and with a physical mixture of phloretin with soya phosphatidylcholine, Span 80 and isopropyl myristate (1:1 w/w). FTIR spectrophotometer model IRAffinity-1S (Shimadzu Corporation, Japan) was used for the analysis in ATR mode at an ambient temperature, using 32 scans and at 4 cm^{-1} resolution, of approximately 5 mg of each sample. The characteristic peaks of pure drug were matched with the physical mixture to check for compatibility. Each analysis was done in triplicate (n=3) [15].

Differential Scanning Calorimetry

The thermal behaviour of phloretin and the presence of drug-excipient interaction was investigated by DSC analysis. Pans with pierced lids (aluminium pans) were accurately weighed (3-5 mg) with empty pan used as a reference and analysed with a differential scanning calorimeter (DSC 4000, PerkinElmer Inc., USA). Onset temperature, peak melting temperature and enthalpy of fusion (ΔH, J/g) were measured under nitrogen purge at 20 mL/min and compared. Triplicate analyses (n=3) were conducted [16].

Solubility Study

The equilibrium solubility of phloretin was studied in solvents and vehicles pertinent to the transethosomal formulation. 5 mL of the different solvents (water, ethanol, PBS pH 7.4, propylene glycol, isopropyl myristate, oleic acid, and Span 80) were each supplemented with excess phloretin (~50 mg) and shaken at 100 rpm, 37 ± 0.5°C, in a water bath shaker (Remi Elektrotechnik Ltd., Model RSB-12, India) for 24 hours. The samples were centrifuged at 3000 rpm (Remi Elektrotechnik Ltd., Model C-24 BL, India), filtered through 0.45 µm membrane filter, diluted with ethanol and quantified spectrophotometricly at λmax 284 nm (LABMAN Scientific Instruments Pvt. Ltd., Model LMSPUV1000B, India). The results are presented as mean ± S.D. (n=3) [17].

Preliminary Trial Batches for Excipient Selection

To select appropriate excipients and determine concentration ranges for Box-Behnken design optimization, six preliminary trial batches of phloretin loaded transethosomes were prepared by the ethanol injection method. The soya phosphatidylcholine and edge activator were dissolved in ethanol at 500 rpm for 15 mins at room temperature and then phloretin was added and completely dissolved. The ethanolic phase was dropwise added to distilled water (30°C) while stirring continuously at 700 rpm for 30 minutes. In the present study the dispersions produced were assessed for vesicle size, PDI, zeta potential and EE. The investigated experimental design (Table 1) was based on outcomes where the independent variables taken were: SPC (2-4% w/v), IPM (0.5-1.5% v/v), and ethanol volume (20-40% v/v) [18].

Table 1: Preliminary Trial Batches for Excipient Screening and Concentration Finalization

Batch	SPC (% w/v)	IPM (% v/v)	Ethanol (% v/v)	Span 80 (% w/v)	Vesicle Size (nm)	PDI	ZP (mV)	%EE
T1	1.0	0.5	20	0.5	312.4 ± 6.2	0.38	−14.2 ± 1.1	54.3 ± 1.8
T2	2.0	0.5	20	0.5	278.6 ± 5.4	0.31	−18.6 ± 0.9	61.7 ± 2.1
T3	2.0	1.0	30	0.5	224.3 ± 4.8	0.27	−21.4 ± 1.3	68.2 ± 1.6
T4	3.0	1.0	30	0.5	198.7 ± 3.9	0.22	−24.8 ± 1.4	74.5 ± 2.3
T5	3.0	1.5	40	0.5	175.2 ± 4.1	0.19	−28.3 ± 1.6	79.8 ± 1.9
T6	4.0	2.0	40	0.5	201.9 ± 5.3	0.26	−22.1 ± 1.2	71.3 ± 2.0

Experimental Design

Design-Expert® software (Version 13.0, Stat-Ease Inc., USA) was used to systematically optimise the transethosomal formulation with a three factor and three level Box-Behnken design (BBD). The independent variables selected were the concentration of SPC (X_1, % w/v), concentration of IPM (X_2, % v/v) and ethanol volume (X_3, % v/v); the responses were vesicle size (Y_1, nm) and entrapment efficiency (Y_2, %). The 17 experimental runs, comprising 5 center point replications, were generated from the design. A quadratic polynomial equation that best fit the responses was:

$$Y = b_0 + b_1X_1 + b_2X_2 + b_3X_3 + b_{12}X_1X_2 + b_{13}X_1X_3 + b_{23}X_2X_3 + b_{11}X_1^2 + b_{22}X_2^2 + b_{33}X_3^2$$

The ANOVA ($p < 0.05$) was used to estimate the significance of the models and contributions of the individual terms and the lack-of-fit test was used to check the model's adequacy. As shown in table 2, the independent variables are coded as X1, X2, X3, and X4. The independent variables used in the Box-Behnken [19].

Table 2: Independent and Dependent Variables for Box-Behnken Design

Factor	Variable	Low Level (-1)	High Level (+1)
X_1	Soya Phosphatidylcholine concentration (% w/v)	2.0	4.0
X_2	Isopropyl Myristate concentration (% v/v)	0.5	1.5
X_3	Ethanol volume (% v/v)	20	40
Response			**Goal**
Y_1	Vesicle Size (nm)		Minimize
Y_2	Entrapment Efficiency (%)		Maximize

Table 3: Box-Behnken Design Formulation Composition (Actual Concentrations)

Run	SPC (% w/v) X_1	IPM (% v/v) X_2	Ethanol (% v/v) X_3	Span 80 (% w/v)	Phloretin (mg)	Water q.s. (mL)
PF1	3	1.5	40	0.5	30	10
PF2	3	1	30	0.5	30	10
PF3	3	1.5	20	0.5	30	10
PF4	3	0.5	40	0.5	30	10
PF5	4	0.5	30	0.5	30	10
PF6	2	1	40	0.5	30	10
PF7	3	1	30	0.5	30	10
PF8	4	1.5	30	0.5	30	10
PF9	4	1	20	0.5	30	10
PF10	3	1	30	0.5	30	10
PF11	3	1	30	0.5	30	10
PF12	3	1	30	0.5	30	10
PF13	4	1	40	0.5	30	10
PF14	2	0.5	30	0.5	30	10
PF15	2	1	20	0.5	30	10
PF16	2	1.5	30	0.5	30	10
PF17	3	0.5	20	0.5	30	10

Preparation of Phloretin-Loaded Transethosomes

The preparation of phloretin loaded transethosomes was done by the ethanol injection method. Accurately weighed amounts of soya phosphatidylcholine (SPC) (as per design concentration), span 80 (0.5% w/v), isopropyl myristate (IPM) (as per design concentration) and phloretin (30 mg) were dissolved in ethanol (as per designated volume) in a glass vial. A magnetic stirrer (Remi Elektrotechnik Ltd., Model 2MLH, India) was used to stir the mixture at 500 rpm for 15 min at 30°C, to get a clear homogeneous ethanolic phase. At the same time distilled water was kept at 30 ± 0.5°C in a water bath (Table 3). An ethanolic phase was slowly fed drop wise through a 21 gauge needle into the aqueous phase under continuous stirring with 700 rpm for 30 minutes at the same temperature. The milky vesicular dispersion was then hydrated further for 60 more minutes with gentle stirring at 30°C. The prepared transethosomes were kept at 4°C for further characterization [20].

Characterization of Phloretin-Loaded Transethosomes

Vesicle Size, Polydispersity Index, and Zeta Potential

The size of vesicles and the PDI and zeta potential of all the transethosomal formulations were determined by dynamic light scattering, obtained with a particle size analyzer (Malvern Panalytical Ltd., Zetasizer Nano ZS, UK). All formulations were diluted 100 times with distilled water before being measured. The size of vesicles and PDI were determined at a scattering angle of 173° and at a temperature of 25°C and zeta potential was measured using electrophoretic light scattering. The data were collected three times (n=3) and presented as mean ± SD [21].

Entrapment Efficiency

The ultracentrifugation method was used to calculate the entrapment efficiency of phloretin. After a 45-minute centrifugation at 15,000 rpm (Remi Elektrotechnik Ltd., Model CR-21, India) at 4°C, transethosomal dispersion (1 mL) was prepared. The supernatant was separated, diluted with ethanol and spectrophotometrically quantified the free drug concentration at λmax 284 nm (LABMAN Scientific Instruments Pvt. Ltd., Model LMSPUV1000B, India). The percentage of CAs that is recovered is called as entrapment efficiency and was calculated as:

$$\%EE = [(\text{Total drug} - \text{Free drug}) / \text{Total drug}] \times 100$$

All measurements were performed in triplicate (n=3) and expressed as mean ± SD [22].

Vesicle Morphology

The optimized transethosomal formulation was analyzed for its surface morphology by the transmission electron microscopy (JEOL Ltd., Model JEM-2100, Japan). A drop of dilute dispersion was placed on a carbon-coated copper grid and allowed to adsorb for 2 minutes, blotted, negatively stained with 2% w/v phosphotungstic acid for 1 minute, and air dried before examination. Appropriate magnification was used in order to evaluate shape, size uniformity and lamellarity of vesicles [23].

Deformability Index

Transethosomal dispersion (1 mL) was conducted through a polycarbonate membrane with a pore size of 200 nm under a constant pressure of 2.5 bar with the mini extruder assembly, and the deformability of the vesicles was evaluated. The extruded dispersion was collected and weighed. The deformability index (D) was determined by:

$$D = J \times (rv / rp)^2$$

The extruded amount (g) is the ratio of the initial size of the vesicles to the mean size of the vesicles after extrusion (rv), which is determined by the membrane pore radius (rp). Triplicate measurements (n=3) were taken for all measurements [24].

In Vitro Drug Release

The dialysis bag diffusion technique was used for in vitro drug release study. A dialysis membrane (MWCO 12000 – 14000 Da) was soaked in PBS (pH 7.4) for 24 hrs and loaded with transethosomal dispersion corresponding to 5 mg phloretin and kept in 50 mL of PBS (pH 7.4) with 0.5% w/v Tween 80 at 37 ± 0.5°C, 100 rpm (Electrolab India Pvt. Ltd., Model TDT-08L, India). Aliquots (1 mL) were removed at 0.5, 1, 2, 4, 6, 8, 12 and 24 h, after which the medium was replaced with fresh medium to ensure sink conditions. The samples were analysed spectrophotometrically at λ_{max} = 284 nm using LABMAN Scientific Instruments Pvt. Ltd. LMSPUV1000B, India. Cumulative percentage drug released was plotted against time and data were fitted to zero order, first order, Higuchi and Korsmeyer–Peppas kinetic models. Experiments were carried out three times (n=3) [25].

Preparation of Phloretin Transethosome-Loaded Nail Lacquer

To prepare a clear lacquer base, ethyl cellulose (EC) was dissolved in ethyl acetate with stirring at 400 rpm for 20 minutes in a magnetic stirrer (Remi Elektrotechnik Ltd., Model 2MLH, India). 20% (v/v) dibutyl phthalate was used as plasticizer and mixed for 10 minutes. The optimized phloretin transethosomal dispersion was added to the lacquer base with gentle stirring (200 rpm) for 20 minutes to ensure even dispersion of the dispersion without vesicle breaking and foaming. Three formulations (NL1, NL2 and NL3) were prepared with different concentrations of EC (5, 7.5 and 10% w/v respectively) and were stored in the amber glass vials at room temperature until evaluated (Table 5) [26].

Table 5: Composition of Phloretin Transethosome-Loaded Nail Lacquer Formulations

Ingredient	NL1	NL2	NL3
Phloretin Transethosomes (mL)	2.0	2.0	2.0
Ethyl Cellulose (% w/v)	5.0	7.5	10.0
Dibutyl Phthalate (% v/v)	20	20	20
Ethyl Acetate q.s. (mL)	10	10	10

Physical Appearance and pH

The formulations of nail lacquer were visually examined to see if they were clear, color, uniform, or phase separated. In order to measure the pH, 0.5 mL of lacquer was dissolved in 10 mL of distilled water, which was measured using a calibrated digital pH meter (Eutech Instruments Pvt. Ltd., Model PC 700, India) using pH 4.0 and 7.0 buffer solutions. All measurements were done in triplicate (n=3) [27].

Drying Time

Each formulation was applied with a brush applicator to a clean glass slide and the amount of time required for the formulation to become completely non-tacky was noted on a stopwatch at 25 ± 2°C and 50 ± 5%RH. All measurements were done in triplicate (n=3) and values were reported as the mean ± SD (s) of seconds [28].

Non-volatile Content

W1 is the accurately weighed quantity of lacquer which was dried at 60°C for 2 hours in a hot air oven (Remi Elektrotechnik Ltd., India) until the constant weight (W_2) was obtained. Non-volatile content was defined as:

Non-volatile content (%) = (W_2 / W_1) × 100

All measurements were performed in triplicate (n=3) and expressed as mean ± SD [29].

Film Adhesion

Evenly applied nail lacquer was dried on bovine nail clippings. The adhesion was checked by using scotch tape and firmly adhering it on the dried film and then peeling it off. The detachment of film was rated as good (no detachment), moderate (partial detachment), and poor (complete detachment). Each experiment was conducted 3 times (n=3) [30].

Ex Vivo Transungual Permeation Study

Bovine hoof membrane (ca. 0.5 mm thick) was placed on a Franz diffusion cell (PermGear Inc., USA) effective diffusion area, 1.77 cm², to study the transungual permeation. Receptor compartment was filled with PBS (pH 7.4) containing 0.5% w/v Tween 80 at 37 ± 0.5°C, 600 rpm. The donor surface was treated with nail lacquer containing 5 mg of phloretin. Samples were taken at intervals of 1, 2, 4, 8, 12, and 24 hours and replaced with fresh PBS, and then analysed at λmax 284 nm (LABMAN Scientific Instruments Pvt. Ltd., Model LMSPUV1000B, India). The permeated amount of accumulated drug (µg/cm²) was plotted as a function of time. The linear slope was used to determine the steady-state flux (Jss) and Kp as:

Kp = Jss / Cd

Where Cd is the donor compartment drug concentration. Each experiment was repeated three times (n=3) [31].

Accelerated Stability Study

A stability test for the optimized NL2 formulation was performed according to ICH Q1A(R2) guidelines with accelerated conditions. The formulation filled in amber glass vials was kept in the stability chamber (Thermolab Scientific Equipments Pvt. Ltd. India Model TLSC-100) at 40°C ± 2°C / 75% RH ± 5% RH for three months. 0, 1, 2 and 3 month samples were tested for physical appearance, pH, drug content, viscosity, drying time, non-volatile content and film adhesion. Each experiment was repeated three times (n=3) and results are reported as mean ± SD [32].

In Vitro Antifungal Activity

The optimized NL2 was tested for antifungal activity against Trichophyton rubrum (ATCC 28188) and *Candida*

albicans (ATCC 10231) using agar well diffusion method. Standardized fungal suspensions (0.5 McFarland, ~1–5 × 10^6 CFU/mL) were inoculated on to SDA plates. Aseptically, wells with a diameter of 8 mm were filled with 100 µL of NL2, 1 mg/mL terbinafine standard (DMSO) or a blank lacquer base (negative control). The pre-diffusion of the plates was done at 4°C for 1 hour and then the plates were incubated for 72 hours at 28 ± 1°C for 48 hours at 37 ± 1°C in incubator (Remi Elektrotechnik Ltd., Model RIS-24 BL Plus, India). Zones of inhibition were determined in millimetres using digital Vernier caliper and reported as mean ± SD (n=3) [33].

RESULTS AND DISCUSSION

RESULTS

Calibration Curve of Phloretin

The calibration curve for phloretin in ethanol was found to be linear between 2 and 12 µg/mL at λmax 284 nm (Figure 1). The absorbance values were found to be directly proportional to concentration and the regression equation showed good linearity with R^2 value. It was determined that the curve was suitable for accurate quantifying of phloretin in all following analytic determinations.

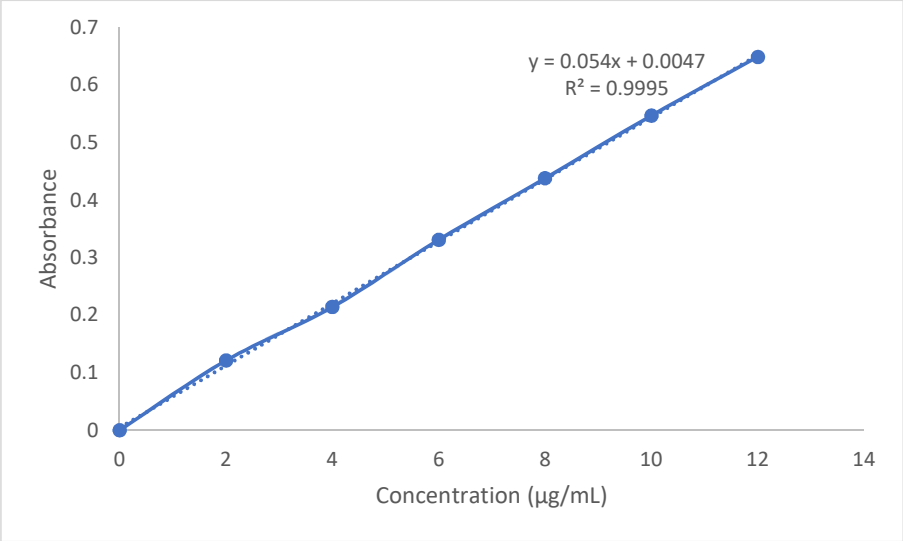

Figure 1: Calibration curve of phloretin in ethanol at λ_{max} 284 nm showing linear relationship between concentration and absorbance

Solubility Studies

Table 6 shows that phloretin is highly lipophilic as it had almost undetectable solubility in water (0.042 ± 0.003 mg/mL) and PBS (0.071 ± 0.004 mg/mL). The maximum solubility was observed in oleic acid (11.47 ± 0.33 mg/mL), followed by Span 80 (9.28 ± 0.24 mg/mL) and isopropyl myristate (8.63 ± 0.29 mg/mL) and these were selected as excipients for transethosomal formulation.

Table 6: Solubility of phloretin in selected solvents and excipients at 37 ± 0.5°C

Solvent / Excipient	Solubility (mg/mL)	Classification
Water	0.042 ± 0.003	Practically Insoluble
Phosphate Buffer Saline (pH 7.4)	0.071 ± 0.004	Practically Insoluble
Ethanol	6.84 ± 0.21	Slightly Soluble
Propylene Glycol	4.12 ± 0.18	Slightly Soluble
Isopropyl Myristate	8.63 ± 0.29	Slightly Soluble
Oleic Acid	11.47 ± 0.33	Sparingly Soluble
Span 80	9.28 ± 0.24	Slightly Soluble

All data are expressed in mean ± SD, (n=3).

FTIR analysis

The ATR-FTIR spectra of phloretin and its physical mixture with the excipients are presented in Figure 2. In the physical mixture with phloretin, all characteristic absorption bands of phloretin (O–H stretch 3409 cm^{-1}, carbonyl C=O stretch 1626.51 cm^{-1}, and aromatic C=C bands) were present, and were only slightly shifted. Absence of drug-excipient interaction was confirmed by a new band at 1737.50 cm^{-1}, which was assigned to IPM ester carbonyl.

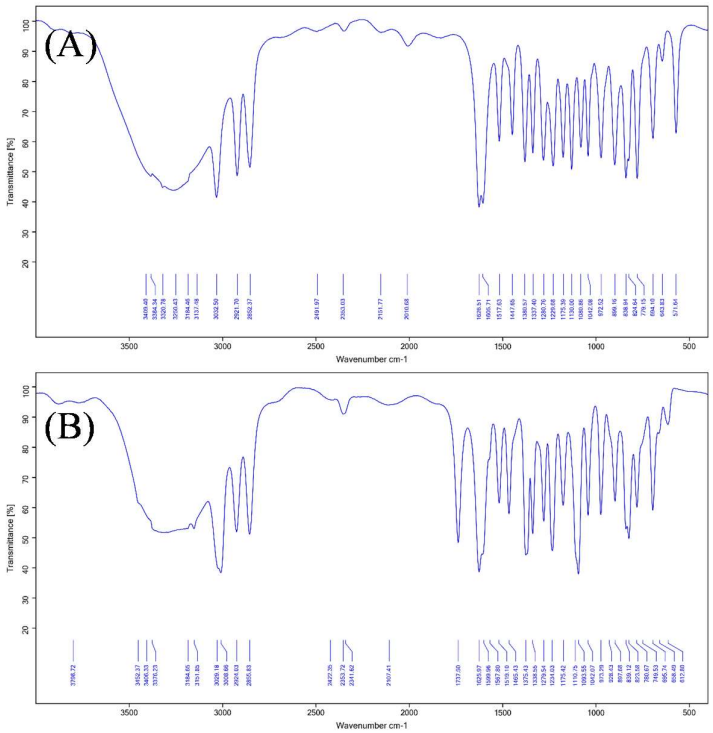

Figure 2: FTIR Spectra of (A) Pure drug and (B) Physical mixture

DSC Analysis

The DSC thermograms of pure phloretin and physical mixture are shown in Figure 3. Pure phloretin showed a strong endothermic melting point peak at 262.33 °C indicating the crystalline purity. No other peaks disappeared or appeared, and a new SPC transition peak at 182.09°C was observed, in addition to the characteristic phloretin endotherm at 262.87°C, confirming the physicochemical compatibility of phloretin with selected excipients in the physical mixture.

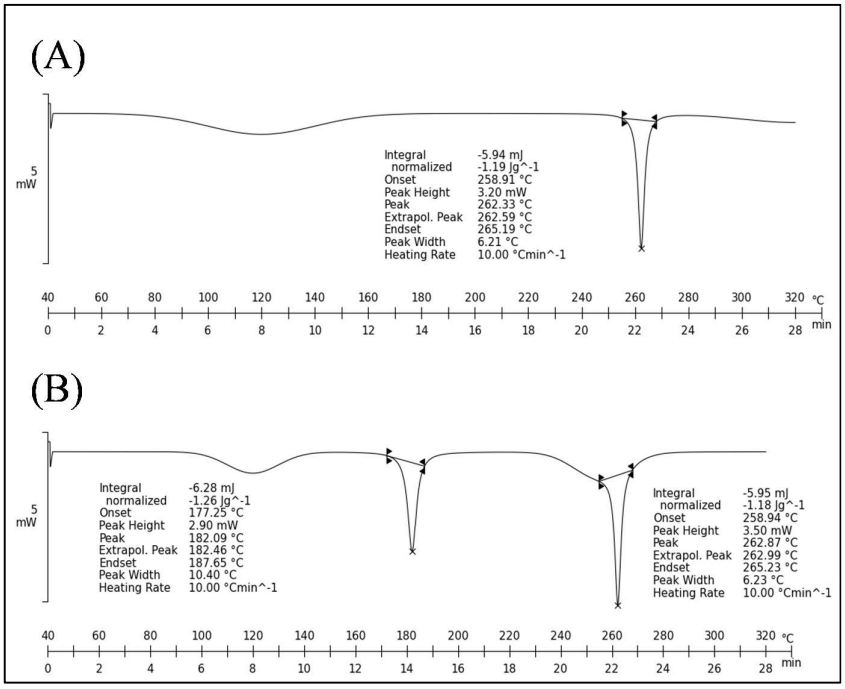

Figure 3: DSC Spectra of (A) Pure drug and (B) Physical mixture

Characterization of Phloretin loaded Transethosomes

The physicochemical characterisation data obtained for all 17 BBD formulations are summarised in Table 7. Vesicle size ranged from 148.9 ± 2.6 nm (PF6) to 241.8 ± 3.9 nm (PF9), PDI from 0.162 to 0.279, and zeta potential from −17.4 to −29.6 mV. The entrapment efficiency was between 65.4% and 77.2%, deformability index was between 1.83 and 3.84, with the highest value of 3.84 ± 0.12 being recorded for PF1.

Table 7: Physicochemical characterization of phloretin-loaded transethosomal formulations PF1–PF17.

Batch	Vesicle Size (nm)	PDI	Zeta Potential (mV)	Entrapment Efficiency (%)	Deformability Index
PF1	163.4 ± 3.2	0.178 ± 0.012	−27.4 ± 1.3	68.7 ± 1.4	3.84 ± 0.12
PF2	197.8 ± 2.9	0.214 ± 0.009	−23.2 ± 0.9	74.3 ± 0.9	2.76 ± 0.09
PF3	201.6 ± 3.7	0.231 ± 0.011	−24.8 ± 1.1	70.2 ± 1.2	2.94 ± 0.11
PF4	184.2 ± 4.1	0.223 ± 0.014	−19.6 ± 1.4	68.1 ± 1.1	2.38 ± 0.14
PF5	234.7 ± 3.8	0.267 ± 0.013	−21.3 ± 1.2	76.8 ± 1.3	2.12 ± 0.13
PF6	148.9 ± 2.6	0.162 ± 0.008	−21.8 ± 1.0	65.4 ± 1.6	3.27 ± 0.10
PF7	196.3 ± 3.1	0.218 ± 0.010	−22.9 ± 1.1	74.1 ± 1.0	2.79 ± 0.10
PF8	214.5 ± 4.4	0.244 ± 0.015	−29.6 ± 1.4	77.2 ± 1.4	3.46 ± 0.13
PF9	241.8 ± 3.9	0.279 ± 0.012	−26.7 ± 1.3	76.4 ± 1.2	1.94 ± 0.11
PF10	198.4 ± 2.7	0.216 ± 0.009	−23.6 ± 0.8	74.8 ± 0.8	2.81 ± 0.08
PF11	197.2 ± 3.3	0.211 ± 0.010	−22.7 ± 1.0	73.6 ± 1.1	2.74 ± 0.09
PF12	199.6 ± 2.8	0.219 ± 0.008	−23.4 ± 0.9	74.6 ± 0.9	2.78 ± 0.10
PF13	208.7 ± 4.2	0.237 ± 0.013	−28.1 ± 1.5	75.3 ± 1.5	3.12 ± 0.12
PF14	178.3 ± 3.4	0.206 ± 0.011	−17.4 ± 1.2	67.1 ± 1.3	1.83 ± 0.11
PF15	186.9 ± 3.6	0.228 ± 0.012	−19.8 ± 1.1	67.9 ± 1.2	2.04 ± 0.12
PF16	158.4 ± 2.9	0.186 ± 0.009	−24.3 ± 1.3	67.4 ± 1.4	3.18 ± 0.11
PF17	219.4 ± 4.6	0.261 ± 0.014	−18.6 ± 1.4	70.8 ± 1.1	1.97 ± 0.13

All data are expressed in mean ± SD, (n=3).

Optimization of phloretin loaded transethosomal formulations

Vesicle Size (Y_1)

The quadratic model for the size of vesicles was highly statistically significant (F-value = 997.27, p-value < 0.0001) and accounted for over 99% of the total variability in the response (R^2 = 0.9992, adjusted R^2 = 0.9982, and predicted R^2 = 0.9965). The signal-to-noise ratio turned out to be very good, as determined by a satisfactory precision of 115.2258. Lack of fit was not significant (p = 0.8033), thus substantiating the model adequacy. The SPC concentration (A) had the highest positive effect (F-value = 5835.95, p < 0.0001), followed by ethanol volume (C) with significant negative effect (F-value = 2360.65, p < 0.0001), and IPM concentration (B) with negative contribution (F-value = 700.24, p < 0.0001) among independent variables. The interaction terms AB, AC and BC were not significant (p > 0.05). The quadratic terms A^2, B^2 and C^2 were all significant (p<0.05), which showed that the surface response was highly curved. The polynomial equation that fits the vesicles size is:

$Y_1 = 197.86 + 28.4A - 9.8375B - 18.0625C - 0.075AB + 1.225AC - 0.75BC + 1.52A^2 - 2.905B^2 - 2.805C^2$

The positive sign of A (+28.4) confirmed that the vesicle dimensions increased with increasing concentrations of SPC, whereas the negative signs of B (−9.8375) and C (−18.0625) showed that the vesicle dimensions decreased with increasing concentrations of IPM and ethanol respectively. These trends were visually confirmed by contour and 3D response surface plots (Figures 4 A1-A3 and 5A1-A3) which showed an increase in vesicle size at increasing concentrations of SPC for all concentration levels of ethanol and IPM, with minimum vesicle size at low SPC and high ethanol and high IPM.

Entrapment Efficiency (Y_2)

The quadratic model was highly significant (F-value = 167.43, p < 0.0001) with R^2 = 0.9954, adjusted R^2 = 0.9894 and predicted R^2 = 0.9775 indicating the reliability of the model. Adequate precision was determined as 38.3286, which showed a good signal to noise ratio. The lack of fit test was non-significant (p = 0.7640) which is an acceptable value for predictive accuracy. The concentration of SPC (A) had the most significant positive influence on entrapment efficiency (F-value = 1116.71, p < 0.0001), whereas ethanol volume (C) had the most significant negative influence (F-value = 47.30, p = 0.0002). The linear effect of IPM concentration (B) was not statistically significant (p = 0.5566). The intercepts AB, AC and BC were not significant (p > 0.05). The quadratic terms B^2 and C^2 were highly significant (p < 0.0001), providing confirmation that the curvature at the extremes of the factors was very strong. The fitted polynomial equation of entrapment efficiency can be written as: $Y_2 = 74.28 + 4.7375A + 0.0875B - 0.975C + 0.025AB + 0.35AC + 0.3BC - 0.1775A^2 - 1.9775B^2 - 2.8525C^2$ The high positive coefficient for A (+4.7375) indicated that SPC concentration was the most significant factor affecting drug encapsulation, while the negative coefficient for C (−0.975) showed that excess ethanol had a deleterious effect on the drug-bilayer structure. Contour and

3D response surface plots (Figures 4 B1-B3 and Figures 5 B1-B3) indicated that the highest EE was obtained at high SPC and low ethanol concentrations, while IPM had a moderate, but non-linear effect over the range of concentrations investigated.

Table 8: Fit Summary of Transethosomal Formulation Responses

Statistical Parameter	Vesicle Size (Y_1)	Entrapment Efficiency (Y_2)
Suggested Model	Quadratic	Quadratic
Standard Deviation	1.05	0.4010
Mean	195.89	71.92
C.V. %	0.5368	0.5575
R^2	0.9992	0.9954
Adjusted R^2	0.9982	0.9894
Predicted R^2	0.9965	0.9775
Adequate Precision	115.2258	38.3286
Lack of Fit (p-value)	0.8033 (NS)	0.7640 (NS)

Table 9: ANOVA Summary for Quadratic Models of Vesicle Size (Y_1) and Entrapment Efficiency (Y_2)

Source	Sum of Squares	df	Mean Square	F-value	p-value	Significance
Vesicle Size (Y_1)						
Model	9923.60	9	1102.62	997.27	< 0.0001	Significant
A-SPC	6452.48	1	6452.48	5835.95	< 0.0001	
B-IPM	774.21	1	774.21	700.24	< 0.0001	
C-Ethanol	2610.03	1	2610.03	2360.65	< 0.0001	
AB	0.0225	1	0.0225	0.0204	0.8906	
AC	6.00	1	6.00	5.43	0.0526	
BC	2.25	1	2.25	2.04	0.1968	
A^2	9.73	1	9.73	8.80	0.0209	
B^2	35.53	1	35.53	32.14	0.0008	
C^2	33.13	1	33.13	29.96	0.0009	
Residual	7.74	7	1.11			
Lack of Fit	1.55	3	0.5158	0.3332	0.8033	Not Significant
Pure Error	6.19	4	1.55			
Cor Total	9931.34	16				
Entrapment Efficiency (Y_2)						
Model	242.29	9	26.92	167.43	< 0.0001	Significant
A-SPC	179.55	1	179.55	1116.71	< 0.0001	
B-IPM	0.0613	1	0.0613	0.3809	0.5566	
C-Ethanol	7.61	1	7.61	47.30	0.0002	
AB	0.0025	1	0.0025	0.0155	0.9043	
AC	0.4900	1	0.4900	3.05	0.1244	
BC	0.3600	1	0.3600	2.24	0.1782	
A^2	0.1327	1	0.1327	0.8251	0.3939	
B^2	16.47	1	16.47	102.41	< 0.0001	
C^2	34.26	1	34.26	213.08	< 0.0001	
Residual	1.13	7	0.1608			
Lack of Fit	0.2575	3	0.0858	0.3955	0.7640	Not Significant
Pure Error	0.8680	4	0.2170			
Cor Total	243.41	16				

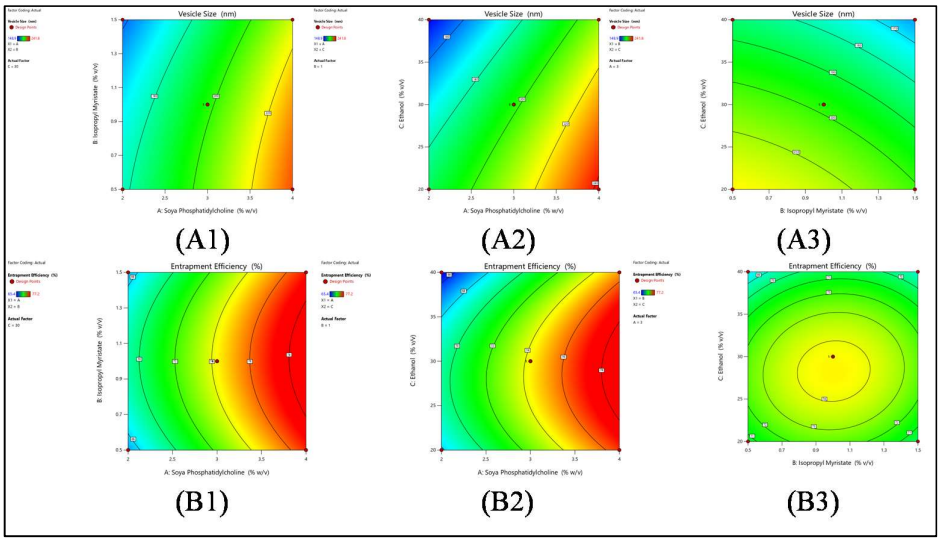

Figure 4: 2D Contour plots showing the effect of formulation variables on critical quality attributes of phloretin-loaded transethosomes. (A1 and B1) Effect of soya phosphatidylcholine concentration (A) and isopropyl myristate concentration (B) on vesicle size (Y_1) and entrapment efficiency (Y_2) respectively; (A2 and B2) effect of soya phosphatidylcholine concentration (A) and ethanol volume (C) on vesicle size (Y_1) and entrapment efficiency (Y_2) respectively; (A3 and B3) effect of isopropyl myristate concentration (B) and ethanol volume (C) on vesicle size (Y_1) and entrapment efficiency (Y_2) respectively.

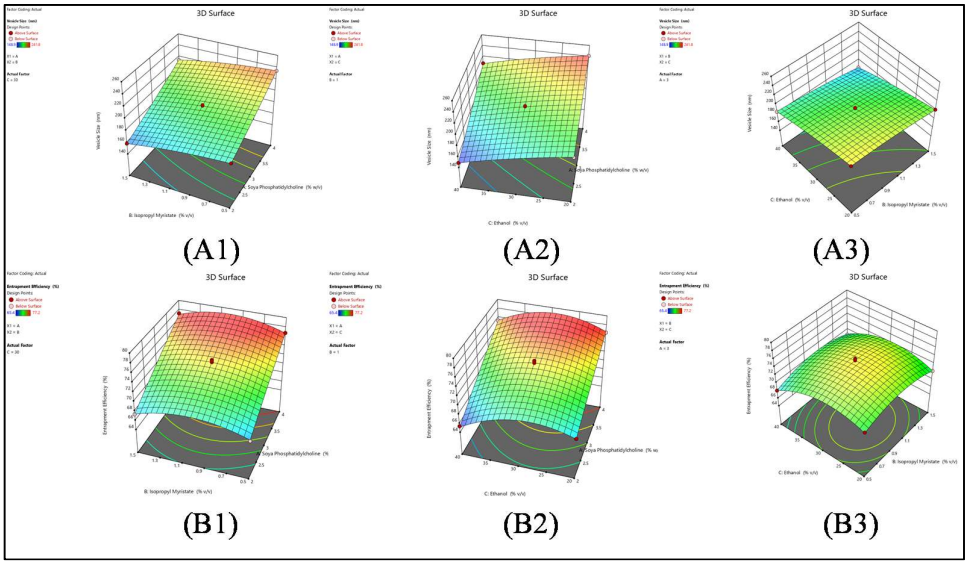

Figure 5: 3D Response surface plots showing the effect of formulation variables on critical quality attributes of phloretin-loaded transethosomes. (A1 and B1) Effect of soya phosphatidylcholine concentration (A) and isopropyl myristate concentration (B) on vesicle size (Y_1) and entrapment efficiency (Y_2) respectively; (A2 and B2) effect of soya phosphatidylcholine concentration (A) and ethanol volume (C) on vesicle size (Y_1) and entrapment efficiency (Y_2) respectively; (A3 and B3) effect of isopropyl myristate concentration (B) and ethanol volume (C) on vesicle size (Y_1) and entrapment efficiency (Y_2) respectively.

Validation of Statistical models

Numerical optimization using desirability function approach identified the optimal formulation at SPC 3.0% w/v, IPM 1.5% v/v, and ethanol 40% v/v with maximum desirability of 1.000 (Table 10). Predicted values of 163.5 nm and 68.86% for vesicle size and entrapment efficiency respectively showed excellent agreement with experimental values of 163.4 nm and 68.7%, yielding negligible percentage bias of 0.061% and 0.241% respectively, confirming robust model predictability.

Table 10: Numerical optimization and validation of the quadratic model - predicted versus experimental values for optimized transethosomal formulation

s	Soya Phosphatidylcholine (% w/v)	Isopropyl Myristate (% v/v)	Ethanol (% v/v)	Vesicle Size (nm)	Entrapment Efficiency (%)	Desirability
Predicted Value	3.00	1.50	40.00	163.5	68.86	1.000
Experimental Value (PF1)	3.00	1.50	40.00	163.4	68.7	-
% Bias	-	-	-	0.061	0.241	-

***In vitro* drug release studies**

The cumulative percent of drug release from all seventeen transethosomal formulations over 12 hours is shown in Figure 6. A characteristic biphasic release pattern was observed in all batches with a moderate burst followed by sustained release. The optimized PF1 showed 87.4 ± 1.8% cumulative release at 12 hours with release ranging from 71.8 ± 1.5% (PF9) to 89.7 ± 1.9% (PF6) at 12 hours, showing a favorable sustained release profile for transungual application.

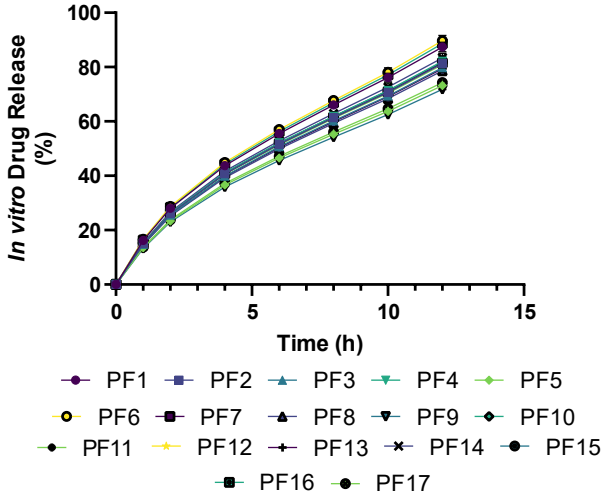

Figure 6: Cumulative percentage in vitro drug release of phloretin from transethosomal formulations PF1-PF17 across 12 hours

Release Kinetics study

The drug release kinetics of optimized PF1 formulation was plotted against five mathematical models as shown in Figure 7. The release exponent n was 0.6260 and the value of R^2 was 0.9993 with the Korsmeyer-Peppas model, defining anomalous non-Fickian diffusion as the release mechanism that predominates. This suggests that both diffusion and breakdown of the vesicles' walls took place, as is typical for phospholipid-based vesicular carrier systems.

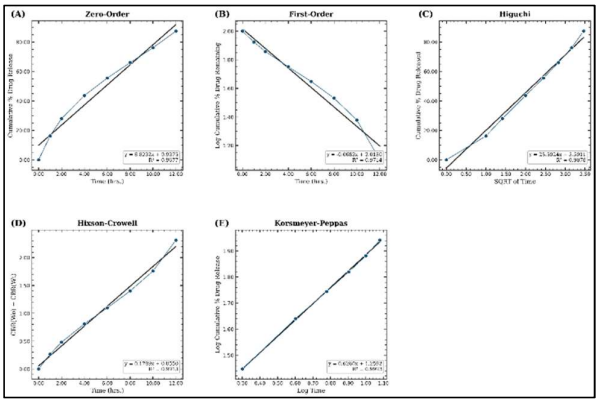

Figure 7: Drug release kinetic plots of optimized phloretin-loaded transethosomal formulation (PF1) fitted to (A) Zero-order, (B) First-order, (C) Higuchi, (D) Hixson-Crowell, and (E) Korsmeyer-Peppas models

TEM analysis

Optimized PF1 formulation (Figure 8) showed the presence of well defined, discrete, spherical vesicles with uniform size distribution and without any sign of appreciable aggregation in TEM image. The phospholipid bilayer that surrounds the electron dense core was suggested to be intact, with the lighter aqueous core. The vesicle size of 163.4 nm obtained from the dynamic light scattering measurements was supported by the observed particle dimensions of the optimized transethosomes using TEM, thus validating the structural integrity of the optimized transethosomes.

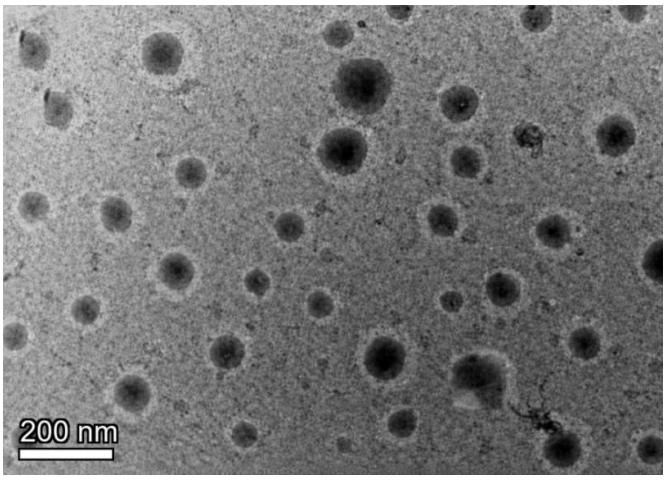

Figure 8: Transmission electron microscopy (TEM) image of optimized phloretin-loaded transethosomal formulation (PF1)

Characterization for Transethosomes loaded Nail Lacquer

The physicochemical characterization data for nail lacquer formulations NL1, NL2 and NL3 are summarized in Table 11. The pH of all the formulations ranged from 4.96 to 5.12 which is within the range of the nail surface physiology. The drying time, viscosity and non-volatile content became higher with increasing amounts of ethyl cellulose, and the film adhesion became higher, while the spreadability became lower, respectively. Finally, NL2 exhibited the most balanced profile having pH 5.08, drug content 97.8%, viscosity of 289.3 cP and film adhesion of 9.87 g/cm², making it the optimized formulation.

Table 11: Physicochemical characterization of phloretin transethosome-loaded nail lacquer formulations NL1, NL2, and NL3

Characterization Parameter	NL1	NL2	NL3
Physical Appearance	Clear, pale yellow, uniform	Clear to slightly opalescent, pale yellow, uniform	Slightly turbid, pale yellow, uniform
Phase Separation	Absent	Absent	Absent
pH	5.12 ± 0.08	5.08 ± 0.11	4.96 ± 0.09
Drying Time (seconds)	68.4 ± 3.2	112.6 ± 4.6	167.3 ± 5.8
Non-volatile Content (%)	18.4 ± 0.6	24.7 ± 0.8	31.2 ± 0.9
Viscosity (cP)	142.6 ± 4.8	289.3 ± 6.2	467.8 ± 8.4
Drug Content (%)	98.4 ± 1.2	97.8 ± 0.9	98.6 ± 1.1
Spreadability (g·cm/s)	38.6 ± 1.4	27.3 ± 1.2	16.8 ± 0.9
Film Adhesion (g/cm²)	6.42 ± 0.28	9.87 ± 0.34	12.64 ± 0.42
Blush Test	Pass	Pass	Pass
Water Resistance (%)	72.4 ± 1.8	84.6 ± 1.6	93.2 ± 1.4

All data are expressed in mean ± SD, (n=3).

***Ex vivo* transungual permeation**

Cumulative transungual permeation profiles of NL1, NL2, and NL3 through bovine hoof membrane over 24 hours are presented in Figure 9 and Table 12. NL1 exhibited the highest cumulative permeation of 81.46 ± 1.92% with Jss of 8.47 µg/cm²/h, followed by NL2 (74.18%, Jss 7.83 µg/cm²/h) and NL3 (54.27%, Jss 6.12 µg/cm²/h). Enhancement ratios of 3.84, 3.54, and 2.77 confirmed significantly superior transungual permeation of transethosomal formulations over conventional delivery.

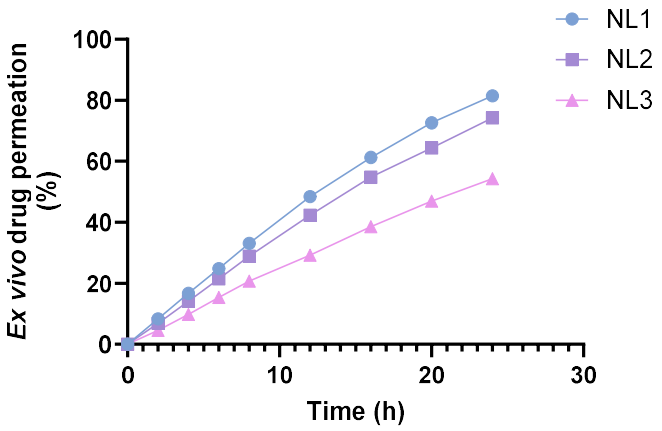

Figure 9: Cumulative percentage *ex vivo* transungual permeation of phloretin from nail lacquer formulations NL1, NL2, and NL3 through bovine hoof membrane at different time intervals.

Table 12: Cumulative percentage *ex vivo* transungual permeation of phloretin from nail lacquer formulations NL1, NL2, and NL3 through bovine hoof membrane at different time intervals.

Time (h)	NL1	NL2	NL3
2	8.34 ± 0.42	6.87 ± 0.36	4.62 ± 0.28
4	16.72 ± 0.68	14.13 ± 0.54	9.84 ± 0.46
6	24.86 ± 0.94	21.47 ± 0.78	15.36 ± 0.62
8	33.14 ± 1.12	28.94 ± 0.96	20.72 ± 0.74
12	48.43 ± 1.38	42.36 ± 1.14	29.18 ± 0.88
16	61.28 ± 1.56	54.82 ± 1.32	38.64 ± 1.04
20	72.64 ± 1.74	64.37 ± 1.48	46.93 ± 1.18
24	81.46 ± 1.92	74.18 ± 1.64	54.27 ± 1.36
Jss (µg/cm²/h)	8.47 ± 0.34	7.83 ± 0.28	6.12 ± 0.31
Kp (×10⁻² cm/h)	1.694 ± 0.07	1.566 ± 0.06	1.224 ± 0.06
Enhancement Ratio	3.84 ± 0.18	3.54 ± 0.14	2.77 ± 0.16
Lag Time (h)	0.84 ± 0.06	1.12 ± 0.08	1.74 ± 0.09

Accelerated Stability study

Accelerated stability data of optimized NL2 stored at 40°C/75% RH for three months are presented in Table 13. The physical appearance did not change during the study period. There was no significant difference in the pH of the samples (5.08 to 5.03), and the amount of drug present ranged from 97.8% to 96.3%, which is still above the 95% acceptance limit. The only minor changes observed were related to viscosity, drying time, non-volatile content, and the adhesion of the film, which all indicated excellent physicochemical stability of NL2.

Table 13: Stability study of optimized phloretin transethosome-loaded nail lacquer (NL2) under accelerated conditions (40°C ± 2°C / 75% RH ± 5% RH) as per ICH Q1A(R2) guidelines.

Parameter	Initial (0 Month)	1 Month	2 Month	3 Month
Physical Appearance	Clear, pale yellow, uniform	Clear, pale yellow, uniform	Clear, pale yellow, uniform	Clear, pale yellow, uniform
pH	5.08 ± 0.11	5.06 ± 0.09	5.04 ± 0.10	5.03 ± 0.12
Drug Content (%)	97.8 ± 0.9	97.2 ± 1.1	96.8 ± 1.0	96.3 ± 1.2
Viscosity (cP)	284.3 ± 6.2	286.1 ± 6.4	287.8 ± 6.6	289.4 ± 6.8
Drying Time (seconds)	112.6 ± 4.6	113.4 ± 4.8	114.2 ± 4.9	115.1 ± 5.1
Non-volatile Content (%)	24.7 ± 0.8	24.4 ± 0.9	24.2 ± 0.8	23.9 ± 0.9
Film Adhesion (g/cm²)	9.87 ± 0.34	9.74 ± 0.36	9.62 ± 0.38	9.48 ± 0.41

All data are expressed in mean ± SD, (n=3).

***In vitro* antifungal activity**

The antifungal efficacy results are shown in Table 14 and Figures 10 and 11. The optimized NL2 showed the zone of inhibition 31.4 ± 1.2 mm and 27.8 ± 0.9 mm against *T. rubrum* and *C. albicans* respectively which was comparable with the standard terbinafine 34.6 ± 1.4 mm and 29.3 ± 1.1 mm respectively. Blank lacquer based was found to be inactive, thus proving that the antifungal activity was totally due to phloretin administered by transethosomal system.

Table 14: *In vitro* antifungal activity of optimized phloretin transethosome-loaded nail lacquer (NL2) and terbinafine against *Trichophyton rubrum* and *Candida albicans* by agar well diffusion method.

Sample	Zone of Inhibition against *T. rubrum* (mm)	Zone of Inhibition against *C. albicans* (mm)
NL2 (Optimized Nail Lacquer)	31.4 ± 1.2	27.8 ± 0.9
Terbinafine (Standard, 1 mg/mL)	34.6 ± 1.4	29.3 ± 1.1
Blank Nail Lacquer Base (Negative Control)	Nil	Nil

All data are expressed in mean ± SD, (n=3).

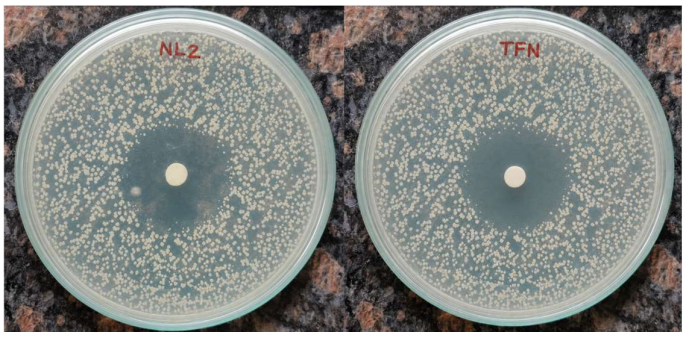

Figure 10: Zone of inhibition of optimized phloretin transethosome-loaded nail lacquer (NL2) and terbinafine (TFN) against *Candida albicans* by agar well diffusion method

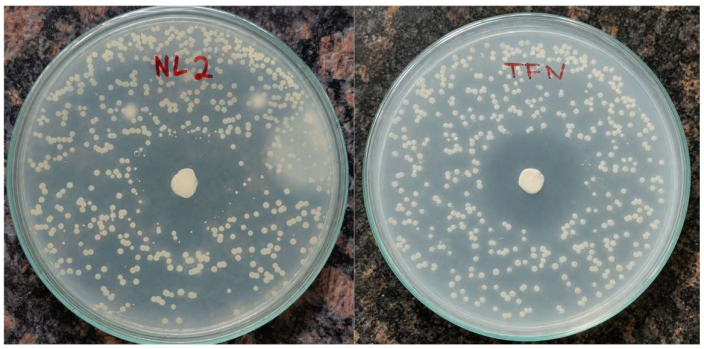

Figure 11: Zone of inhibition of optimized phloretin transethosome-loaded nail lacquer (NL2) and terbinafine (TFN) against *Trichophyton rubrum* by agar well diffusion method

DISCUSSION

In the present study, the transethosomes containing phloretin were successfully developed and optimized for an ethyl cellulose based nail lacquer for delivery of phloretin to nail to treat onychomycosis. The phloretin was found to possess similar physicochemical characteristics in terms of λ_{max} (284 nm) in preformulation investigations, which are in agreement with the reported UV absorption properties of dihydrochalcone compounds [34]. The physicochemical compatibility of phloretin and selected excipients was confirmed by FTIR and DSC analysis (Figures 2 and 3), which showed no physicochemical interactions with the resulting appearance of new peaks and complete superimposition of the drug peaks in the physical mixture. Compatibility profiles, similar to those reported for the formulation of flavonoid-loaded vesicular systems [35], were obtained. Based on the solubility data as shown in Table 6, there was good drug solubility in isopropyl myristate (8.63mg/mL) and Span 80 (9.28mg/mL) which made these two excipients to be incorporated as functionally active excipients which acted simultaneously in both drug solubilization and vesicle deformability; a strategy consistent to the dual function, edge activator approaches described in recent transungual vesicular delivery literature [36]. After Box-Behnken design optimization, the quadratic model was well fitted for both responses with R^2 values both

over 0.995 and with no significant lack of fit (Tables 8 and 9), which showed a good predictive ability. The concentration of SPC emerged as the major factor that influenced both vesicle size and entrapment efficiency in agreement with previously reported for phospholipid based vesicular systems that showed a greater drug entrapment efficiency with higher phospholipid concentration, thereby increasing the mass of bilayer available for the entrapment of the drug [37]. An increase in ethanol volume also affected the entrapment efficiency, consistent with what was reported by Nair et al., who showed that higher ethanol level results in more leakage of the drugs from the membrane and thus affects the integrity of the bilayer structure. The vesicles formed by the optimized formulation PF1 had a size of 163.4 nm and entrapment efficiency of 68.7% [38]. The value of the deformability index was 3.84, which is high, indicating that the vesicles are highly deformable and can be squeezed through narrow capillaries in the retina, thereby avoiding damage to the retina.

The percentage bias was very low between the predicted and experimental values, as shown in Table 10, which confirmed the reliability of the statistical model. The in vitro drug release profile of PF1 (87.4 ± 1.8% at 12 hours) was biphasic with the Korsmeyer-Peppas model having n = 0.6260, which suggested anomalous non-Fickian diffusion mechanism of drug release involving a combination of vesicular membrane diffusion and gradual bilayer erosion as widely reported in the literature for ultra-deformable phospholipid vesicular carriers [39]. TEM analysis (Figure 8) verified discrete spherical morphology and intact bilayer structure which is consistent with TEM characterization of transethosomes in similar studies [40]. Three formulations with varying concentrations of ethyl cellulose (EC) were prepared by incorporating the optimized phloretin transethosomes into the ethyl cellulose-based nail lacquer (Table 11) with the most favorable balance of the physicochemical properties being obtained with NL2 (7.5% of EC). The film forming behavior of nail lacquer formulations of ethyl cellulose as observed by the present researchers by increasing EC concentration in the lacquer formulation shows increase in viscosity (142.6 to 467.8 cP), drying time (68.4 to 167.3 s), film adhesion (6.42 to 12.64 g/cm²) and water resistance (72.4 to 93.2%) which are in accordance with the reported polymer concentration dependent film forming behavior of ethyl cellulose nail lacquer system [41].

The range of pH (4.96-5.12) of all formulations is in line with the physiological nail surface pH (4.5-5.5) and reduces the potential irritation when applied repeatedly [42]. In the ex vivo transungual permeation studies conducted using bovine hoof membrane, the steady state flux of NL2 was found to be 7.83 µg/cm2h with an enhancement ratio of 3.54 (Figure 9) which was significantly higher than the nail lacquer permeation values reported in literature (1.5 to 2.5 µg/cm2h) for conventional nail lacquer formulations [43]. The squeeze mechanism of the ultradeformable vesicles traversing the nail keratin matrix, under the gradient of transungual hydration, as described by Nair et al. and Pund et al. for deformable vesicular transungual systems was responsible for the superior permeation enhancement obtained from the transethosomal nail lacquer. The results of in vitro antifungal activity evaluation showed that NL2 exhibited zones of inhibition of 31.4 ± 1.2 mm and 27.8 ± 0.9 mm against T. rubrum and C. albicans, respectively, which is comparable with the terbinafine standard value (34.6 ± 1.4 mm and 29.3 ± 1.1 mm). This implies that the phloretin from NL2 has the potential to inhibit the growth of dermatophytes and *C. albicans*, consistent with the reported antifungal activity of phloretin against *C. albicans* and dermatophytes due to its ability to disrupt ergosterol biosynthesis and impair fungal membrane integrity [44]. The accelerated stability testing per ICH Q1A(R2) guideline confirmed the NL2 formulation to be suitable for practical therapeutic use in the treatment of onychomycosis as all the physicochemical integrity parameters were found to be within the acceptable limits after three months of testing at 40°C/75%RH with drug content remaining above 96% (Table 13).

CONCLUSION

The present study successfully proved the feasibility of phloretin loaded transethosomes embedded in the ethyl cellulose base nail lacquer to be used as a possible transungual drug delivery system for the treatment of onychomycosis. Optimized transethosomes (Box-Behnken design) SPC 3% w/v, IPM 1.5% v/v and ethanol 40% v/v showed vesicles size 163.4 nm, entrapment efficiency of 68.7% and high deformability index of 3.84, while the optimized NL2 formulation showed excellent physicochemical stability for 3 months under accelerated conditions, sustained drug release and significant antifungal activity against Trichophyton rubrum and Candida albicans comparable to terbinafine, with the enhancement ratio of transungual permeation of 3.54. It brings clinically relevant benefits such as site-specific delivery of a drug, reduced systemic side-effects caused by oral anti-fungal drugs, and ease of application at the site leading to better patient compliance with topical therapy. The promising results suggest that this innovative transungual delivery system has potential for further research and development into its full therapeutic capabilities using in vivo pharmacokinetic and pharmacodynamic studies.

DECLARATIONS

Funding

The authors received no financial support for the research, authorship, or publication of this article.

Ethics Declaration

No human participants or live animals were involved in this study. Bovine hoof membranes were obtained from a government-approved slaughterhouse and used only for ex vivo permeation studies. Therefore, ethical approval was not required.

Conflict of Interest

The authors declare that they have no conflict of interest.

ABBREVIATIONS

SPC: Soya Phosphatidylcholine; IPM: Isopropyl Myristate; BBD: Box-Behnken Design; PDI: Polydispersity Index; ZP: Zeta Potential; EE: Entrapment Efficiency; FTIR: Fourier Transform Infrared Spectroscopy; ATR: Attenuated Total Reflectance; DSC: Differential Scanning Calorimetry; TEM: Transmission Electron Microscopy; DLS: Dynamic Light Scattering; UV: Ultraviolet; λmax: Wavelength of Maximum Absorbance; PBS: Phosphate Buffer Saline; MWCO: Molecular Weight Cut-Off; EC: Ethyl Cellulose; DBP: Dibutyl Phthalate; ANOVA: Analysis of Variance; df: Degrees of Freedom; R^2: Coefficient of Determination; CV: Coefficient of Variation; Jss: Steady-State Flux; Kp: Permeability Coefficient; ICH: International Council for Harmonisation; RH: Relative Humidity; SDA: Sabouraud Dextrose Agar; DMSO: Dimethyl Sulfoxide; CFU: Colony Forming Units; ATCC: American Type Culture Collection; MTCC: Microbial Type Culture Collection; MW: Molecular Weight; SD: Standard Deviation.

REFERENCES

1. Lee DK, Lipner SR. Optimal diagnosis and management of common nail disorders. Annals of Medicine 2022;54:694–712. https://doi.org/10.1080/07853890.2022.2044511.
2. Falotico JM, Lipner SR. Updated Perspectives on the Diagnosis and Management of Onychomycosis. Clinical, Cosmetic and Investigational Dermatology 2022;15:1933–57. https://doi.org/10.2147/CCID.S362635.
3. Albucker SJ, Falotico JM, Choo Z-N, Matushansky JT, Lipner SR. Risk Factors and Treatment Trends for Onychomycosis: A Case–Control Study of Onychomycosis Patients in the All of Us Research Program. Journal of Fungi 2023;9:712. https://doi.org/10.3390/jof9070712.
4. Gupta AK, Wang T, Polla Ravi S, Mann A, Bamimore MA. Global prevalence of onychomycosis in general and special populations: An updated perspective. Mycoses 2024;67:e13725. https://doi.org/10.1111/myc.13725.
5. Piraccini BM, Starace M, Rubin AI, Di Chiacchio NG, Iorizzo M, Rigopoulos D, et al. Onychomycosis: Recommendations for Diagnosis, Assessment of Treatment Efficacy, and Specialist Referral. The CONSONANCE Consensus Project. Dermatol Ther (Heidelb) 2022;12:885–98. https://doi.org/10.1007/s13555-022-00698-x.
6. Shelke V, Kale A, Kulkarni YA, Gaikwad AB. Phloretin: a comprehensive review of its potential against diabetes and associated complications. J Pharm Pharmacol 2024;76:201–12. https://doi.org/10.1093/jpp/rgae010.
7. Tuli HS, Rath P, Chauhan A, Ramniwas S, Vashishth K, Varol M, et al. Phloretin, as a Potent Anticancer Compound: From Chemistry to Cellular Interactions. Molecules 2022;27:8819. https://doi.org/10.3390/molecules27248819.
8. Habtemariam S. The Molecular Pharmacology of Phloretin: Anti-Inflammatory Mechanisms of Action. Biomedicines 2023;11:143. https://doi.org/10.3390/biomedicines11010143.
9. Nakhate KT, Badwaik H, Choudhary R, Sakure K, Agrawal YO, Sharma C, et al. Therapeutic Potential and Pharmaceutical Development of a Multitargeted Flavonoid Phloretin. Nutrients 2022;14:3638. https://doi.org/10.3390/nu14173638.
10. Aodah AH, Hashmi S, Akhtar N, Ullah Z, Zafar A, Zaki RM, et al. Formulation Development, Optimization by Box–Behnken Design, and In Vitro and Ex Vivo Characterization of Hexatriacontane-Loaded Transethosomal Gel for Antimicrobial Treatment for Skin Infections. Gels 2023;9:322. https://doi.org/10.3390/gels9040322.
11. Gupta V, Joshi NK. Formulation, Development and Evaluation of Ketoprofen Loaded Transethosomes Gel. Journal of Drug Delivery & Therapeutics 2022;12:86. https://doi.org/10.22270/jddt.v12i1.5177.
12. Patel UD, Mastiholimath VS. Formulation Optimization and Characterization of Bifonazole-Loaded Transethosomal Gel by 32 Factorial Design for the Treatment of Topical Fungal Infection. BioNanoSci 2025;15:486. https://doi.org/10.1007/s12668-025-02109-9.
13. Munir M, Ahmad S, Jamshaid T, Hameed H, Zaman M, Jamshaid U, et al. Lornoxicam Loaded Transethosomal Gel: Formulation, Box-Behnken Optimization, Ex-Vivo and In-Vivo Characterization. J Pharm Innov 2026;21:448. https://doi.org/10.1007/s12247-026-10609-8.
14. Alfadhel MM, Zaki RM, Aldosari BN, Sayed OM. Numerical Optimization of Prednisolone–Tacrolimus Loaded Ultraflexible Transethosomes for Transdermal Delivery Enhancement; Box–Behnken Design, Evaluation, Optimization, and Pharmacokinetic Study. Gels 2023;9:400. https://doi.org/10.3390/gels9050400.
15. Bin Jardan YA, Ahad A, Raish M, Al-Jenoobi FI. Preparation and Characterization of Transethosome Formulation for the Enhanced Delivery of Sinapic Acid. Pharmaceutics 2023;15:2391. https://doi.org/10.3390/pharmaceutics15102391.
16. Veer PJ, Mastiholimath VS. Formulation, Characterization, and Optimization of Transethosomes for Enhanced Transdermal Delivery of Methotrexate. J Pharm Innov 2023;18:2385–401. https://doi.org/10.1007/s12247-023-09799-2.

17. Bevinakoppamath SS, Dandagi PM, Hulyalkar S, Biradar P. Formulation, Evaluation and Optimization of Acitretin Loaded Transethosomes for the Management of Psoriasis. J Pharm Innov 2024;19:51. https://doi.org/10.1007/s12247-024-09864-4.
18. Zaki RM, Seshadri VD, Mutayran AS, Elsawaf LA, Hamad AM, Almurshedi AS, et al. Wound Healing Efficacy of Rosuvastatin Transethosomal Gel, I Optimal Optimization, Histological and In Vivo Evaluation. Pharmaceutics 2022;14:2521. https://doi.org/10.3390/pharmaceutics14112521.
19. Ali F, Ali A, Sultana N, Waheed A, Jahan S, Aqil M, et al. Tailoring and Evaluation of Berberine Loaded Transethosomal Gel for Effective Transdermal Delivery: Optimization, Characterization, and in vitro Evaluation. J Clust Sci 2024;35:1761–76. https://doi.org/10.1007/s10876-024-02616-x.
20. Adnan M, Afzal O, S. A. Altamimi A, Alamri MA, Haider T, Faheem Haider Md. Development and optimization of transethosomal gel of apigenin for topical delivery: In-vitro, ex-vivo and cell line assessment. International Journal of Pharmaceutics 2023;631:122506. https://doi.org/10.1016/j.ijpharm.2022.122506.
21. Alam P, Imran M, Jahan S, Akhtar A, Hasan Z. Formulation and Characterization of Hesperidin-Loaded Transethosomal Gel for Dermal Delivery to Enhance Antibacterial Activity: Comprehension of In Vitro, Ex Vivo, and Dermatokinetic Analysis. Gels 2023;9:791. https://doi.org/10.3390/gels9100791.
22. Kokatanur UA, Dandagi PM, Patil S. QbD-guided development of a simvastatin-loaded transethosomal gel for enhanced transdermal delivery: optimization, characterization, and in vivo antihyperlipidemic evaluation. Drug Development and Industrial Pharmacy 2026;52:104–22. https://doi.org/10.1080/03639045.2025.2586232.
23. Alyami MH, Alyami HS, Abdo AM, A. Sabry S, El-Nahas HM, Ayoub MM. Maximizing the Use of Ivermectin Transethosomal Cream in the Treatment of Scabies. Pharmaceutics 2024;16:1026. https://doi.org/10.3390/pharmaceutics16081026.
24. Mammella A, Bhavana V, Chary PS, Anuradha U, Mehra NK. Modulation of chondroprotective hyaluronic acid and poloxamer gel with Ketoprofen loaded transethosomes: Quality by design-based optimization, characterization, and preclinical investigations in osteoarthritis. International Journal of Biological Macromolecules 2024;280:135919. https://doi.org/10.1016/j.ijbiomac.2024.135919.
25. Rehman M, Sohail S, Ali Z, Alamri AH, Lahiq AA, Alqahtani T, et al. Development and optimization of cilostazol loaded transethosomal gel for improved performance. Pharmaceutical Development and Technology 2025;30:821–39. https://doi.org/10.1080/10837450.2025.2521055.
26. Patil S, Dandagi PM, Kazi T, Hulyalkar S, Biradar P, Kumbar V. A DoE-based development and characterization of Nadifloxacin-loaded transethosomal gel for the treatment of Acne vulgaris. Futur J Pharm Sci 2024;10:46. https://doi.org/10.1186/s43094-024-00616-2.
27. Dehari D, Mehata AK, Priya V, Parbat D, Kumar D, Srivastava AK, et al. Luliconazole Nail Lacquer for the Treatment of Onychomycosis: Formulation, Characterization and In Vitro and Ex Vivo Evaluation. AAPS PharmSciTech 2022;23:175. https://doi.org/10.1208/s12249-022-02324-7.
28. Diptee Marchande. Formulation and Evaluation of Medicated Nail Lacquer for the Treatment of Onychomycosis 2024. https://doi.org/10.5281/ZENODO.13294084.
29. Goyal R, Goyal A, Khan AA, Fatima S, Singh T, Malik DS. Formulation and evaluation of herbal essential oil based nail lacquer for management of onychomycosis. Journal of Medical Mycology 2024;34:101515. https://doi.org/10.1016/j.mycmed.2024.101515.
30. Scandorieiro S, de Oliveira NR, de Souza M, de Castro-Hoshino LV, Baesso ML, Nakazato G, et al. Nail Lacquer Containing Origanum vulgare and Rosmarinus officinalis Essential Oils and Biogenic Silver Nanoparticles for Onychomycosis: Development, Characterization, and Evaluation of Antifungal Efficacy. Antibiotics 2024;13:892. https://doi.org/10.3390/antibiotics13090892.
31. Patil A, Chavan H, Tekade DB. Formulation And Evaluation of Antifungal Nail Lacquer for Treatment of Onychomycosis. International Journal of Scientific Research and Technology 2024;02:107–15. https://doi.org/10.5281/zenodo.14362171.
32. Pradhan PT, Panigrahi A, Ray J, Dash RS, Pattnaik G, Sahu A, et al. Development and Characterization of Ketoconazole-Loaded Nail Lacquer for the Topical Treatment of Onychomycosis. Journal of Young Pharmacists 2025;17:604. https://doi.org/10.5530/jyp.20251665.
33. Gizaw A, Marami LM, Teshome I, Sarba EJ, Admasu P, Babele DA, et al. Phytochemical Screening and In Vitro Antifungal Activity of Selected Medicinal Plants against Candida albicans and Aspergillus niger in West Shewa Zone, Ethiopia. Advances in Pharmacological and Pharmaceutical Sciences 2022;2022:3299146. https://doi.org/10.1155/2022/3299146.

34. Abdallah MH, Elghamry HA, Khalifa NE, Khojali WMA, Khafagy E-S, Shawky S, et al. Development and Optimization of Erythromycin Loaded Transethosomes Cinnamon Oil Based Emulgel for Antimicrobial Efficiency. Gels 2023;9:137. https://doi.org/10.3390/gels9020137.
35. Ashraf F, Idrees HA, Munir M, Ajmal M. Development and optimization of mirtazapine loaded lipid-based transethosomal gel; in-vitro, ex-vivo and toxicological analysis. Pakistan Journal of Pharmaceutical Sciences 2026;39:1295. https://doi.org/10.36721/PJPS.2026.39.5.REG.14153.1.
36. Bobade PS, Mishra AS, Ganorkar SB, Telange DR, Chalikwar SS. QbD-Anchored Preparation and Assessment of Transethosomal Gel for Enhanced Skin Permeation of Tamoxifen Citrate. Current Pharmaceutical Design 2025;31:2352–69. https://doi.org/10.2174/0113816128344198250308022732.
37. Mishra KK, Kaur CD, Gupta A. Development of itraconazole loaded ultra-deformable transethosomes containing oleic-acid for effective treatment of dermatophytosis: Box-Behnken design, ex-vivo and in-vivo studies. Journal of Drug Delivery Science and Technology 2022;67:102998. https://doi.org/10.1016/j.jddst.2021.102998.
38. Jaikham P, Leelapornpisid P, Tragoolpua K, Koonyosying P, Lin W-C, Poomanee W. Transethosomes-encapsulated Bouea macrophylla seed extract for anti-acne application: Formulation optimization, antibacterial efficacy, and safety assessment. Journal of Agriculture and Food Research 2025;20:101764. https://doi.org/10.1016/j.jafr.2025.101764.
39. Dongsar TS, Dongsar TT, Alsayari A, Wahab S, Garima Gupta, Kesharwani P. Gallic Acid-Loaded Transethosomal Gel for Enhanced Topical Delivery and Sustained Therapeutic Efficacy in Psoriasis Management: Formulation, Optimization, In Vitro and Ex Vivo Assessment. AAPS PharmSciTech 2025;26:183. https://doi.org/10.1208/s12249-025-03179-4.
40. Mishra K, Kaur C. Screening of process variables using Box–Behnken design in the fabrication of berberine hydrochloride-loaded transethosomes for enhanced transdermal delivery. The Thai Journal of Pharmaceutical Sciences 2022;46:191–202. https://doi.org/10.56808/3027-7922.2561.
41. Singh G, Narang RK. Quality by Design Assisted Development of Luliconazole Transethosomes in Gel for the Management of Candida albicans Infection. ASSAY and Drug Development Technologies 2024;22:1–17. https://doi.org/10.1089/adt.2023.059.
42. Allizond V, Cavallo L, Roana J, Mandras N, Cuffini AM, Tullio V, et al. In Vitro Antifungal Activity of Selected Essential Oils against Drug-Resistant Clinical Aspergillus spp. Strains. Molecules 2023;28:7259. https://doi.org/10.3390/molecules28217259.
43. Quindós G, Miranda-Cadena K, San-Millán R, Borroto-Esoda K, Cantón E, Linares-Sicilia MJ, et al. In Vitro Antifungal Activity of Ibrexafungerp (SCY-078) Against Contemporary Blood Isolates From Medically Relevant Species of Candida: A European Study. Front Cell Infect Microbiol 2022;12. https://doi.org/10.3389/fcimb.2022.906563.
44. Nikhath M, S S. Formulation and Evaluation of Nail Drug Delivery System of Anti Fungal Drug. Asian Journal of Pharmaceutical Research and Development 2022;10:44–52. https://doi.org/10.22270/ajprd.v10i6.1189.